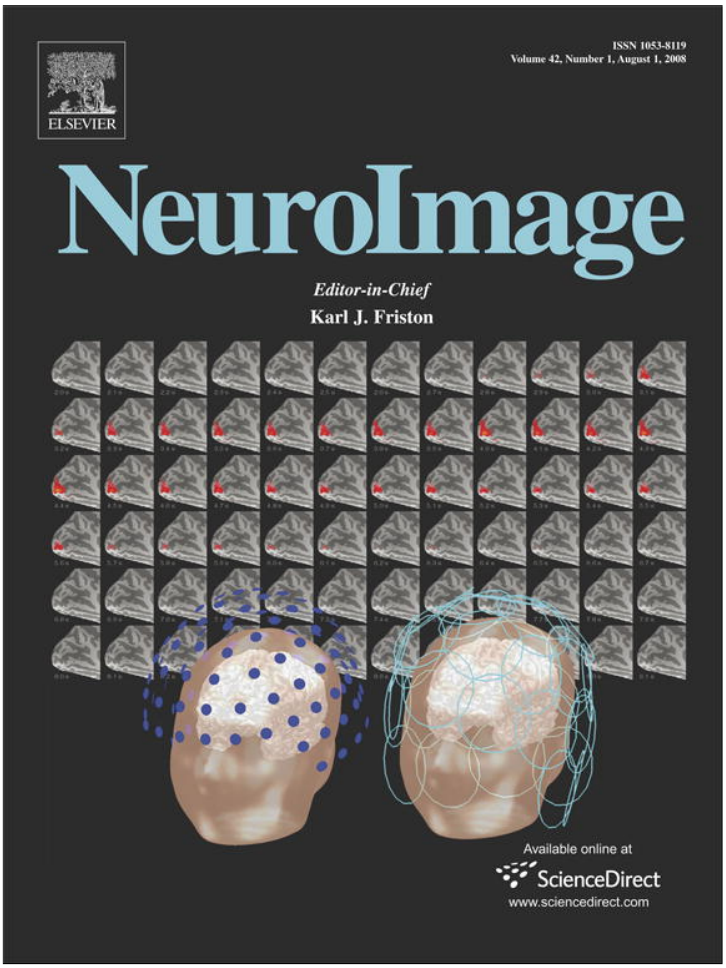

ELSEVIER

NeuroImage

www.elsevier.com/locate/ynimg
NeuroImage 42 (2008) 60–69

High resolution three-dimensional brain atlas using an average magnetic resonance image of 40 adult C57Bl/6J mice

A.E. Dorr,[a] J.P. Lerch,[b] S. Spring,[b] N. Kabani,[a,*,1] and R.M. Henkelman[b,1]

[a]*Clinical Integrative Biology, Sunnybrook Health Sciences Centre, Toronto ON, Canada*
[b]*Mouse Imaging Centre, Hospital for Sick Children, Toronto Centre for Phenogenomics, Toronto ON, Canada*

Received 30 November 2007; revised 26 February 2008; accepted 16 March 2008
Available online 8 April 2008

Detailed anatomical atlases can provide considerable interpretive power in studies of both human and rodent neuroanatomy. Here we describe a three-dimensional atlas of the mouse brain, manually segmented into 62 structures, based on an average of 32 μm isotropic resolution T_2-weighted, within skull images of forty 12 week old C57Bl/6J mice, scanned on a 7 T scanner. Individual scans were normalized, registered, and averaged into one volume. Structures within the cerebrum, cerebellum, and brainstem were painted on each slice of the average MR image while using simultaneous viewing of the coronal, sagittal and horizontal orientations. The final product, which will be freely available to the research community, provides the most detailed MR-based, three-dimensional neuroanatomical atlas of the whole brain yet created. The atlas is furthermore accompanied by ancillary detailed descriptions of boundaries for each structure and provides high quality neuroanatomical details pertinent to MR studies using mouse models in research.

Introduction

High resolution magnetic resonance imaging (MRI) has recently seen increased use in mouse phenotyping studies (Redwine et al., 2003; Bock et al., 2006; Badea et al., 2007b) as reviewed in Nieman et al. (2005) and Anderson and Frank (2007). MRI provides detailed neuroanatomical information covering the whole brain and, in combination with advanced image processing, can rapidly localize regions of the cerebrum differing by genotype. The use of structural segmentations can enhance analyses by (1) aiding in localizing statistical peaks and (2) providing tissue volumes for those structures. Creating a detailed three-dimensional atlas of the brain from MRI is, however, not a trivial task, requiring detailed understanding of the underlying anatomy along with high-resolution MR scans upon which to base the segmentation.

To date, a few structural murine brain atlases have been created with the aid of MRI on neonatal and postnatal mice; each study using differing methodologies and characteristics. Table 1 summarizes the studies conducted previously in creating mouse brain atlases and gives a concise comparison of our present work with those of other investigators. Using this table of previous murine brain MR studies we can conclude the following: (1) higher resolution and signal to noise ratio (SNR), as should be obvious, allow a greater number of anatomical details to be discerned; (2) fixed brain MRI provides greater detail than in-vivo as reviewed in Benveniste and Blackband (2006); (3) removing brains from the skull for ex-vivo scanning distorts the underlying anatomy (Kovacevic et al., 2005; Ma et al., 2005); and (4), using a model independent average of a population of mice rather than one individual allows for the capture of within strain variance and provides greater SNR (Kovacevic et al., 2005). These points are elaborated upon in the Discussion section of this paper.

The present study provides an atlas, based on the commonly used C57Bl/6J mouse, which complements and improves on previous works in this field. The novelty of this work is represented by a manually segmented atlas based on 32 μm^3 resolution images created from average MRI of 40 mouse brains: 20 male and 20 female at 12 weeks in age. A total of 62 brain structures which could be clearly visualized at this resolution was manually traced on each slice. These, to the best of our knowledge, are the most number of neuroanatomical structures manually segmented on a mouse average MRI. We show three-dimensional representations of complex brain relationships that can be directly visualized using our atlas. This atlas will be freely available (http://www.mouseimaging.ca/research/mouse_atlas.html) to the research community and the Supplementary data of this paper will provide the users with the detailed descriptions of the boundaries for each structure.

Materials and methods

The mice used in this study were chosen to be 12 week old since this is the most common age group used in behavioural and

* Corresponding author. Clinical Integrative Biology, Sunnybrook Health Sciences Centre, 2075 Bayview Avenue, Room E-238 Toronto, ON, Canada M4N 3M5. Fax: +1 416 480 4892.
E-mail address: nkabani@sten.sunnybrook.utoronto.ca (N. Kabani).
[1] Senior authorship on this paper is equally shared by Drs. Kabani and Henkelman.

Available online on ScienceDirect (www.sciencedirect.com).

1053-8119/$ - see front matter © 2008 Elsevier Inc. All rights reserved.
doi:10.1016/j.neuroimage.2008.03.037

Table 1
Comparison of MR-based mouse atlases from various groups and the present study

	MacKenzie-Graham et al., 2004	Kovacevic et al., 2005	Ma et al., 2005	Lee et al., 2005	Ali et al., 2005	Bock et al., 2006	Chen et al., 2006	Dorr et al., 2007	Sharief et al., 2008	Badea et al., 2007a,b	Present study
Strains	C57Bl/6J	129Sl/Svlm J	C57Bl/6J	C57Bl/6J	C57Bl/6J	Cdf/cdf, cdf/+ and +/+	129Sl/Svlm J, C57Bl/6J, and CD1	CBA	C57Bl/6J and BXD	C57Bl/6J	C57Bl/6J
Resolution MR (T2)	60 μm^3	60 μm^3	47 μm^3	Up to 40 μm^3	90 μm^3	156 μm^3	60 μm^3	32 μm^3	43 μm^3	43 μm^3	32 μm^3
N	No info	9 male	10 male	8 (mixed gender)	6 male	15 (mixed gender)	27 male	4 male	12 male	6 (unspecified)	20 male, 20 female
Modalities	MR, histology, blockface, and inmmuno-histochem	MR	MR only	MR	MR	MR and histology	MR	MR and CT	MR	MR	MR
Average MR used	No	Yes	Yes	Yes	No	Yes	Yes	Yes	No	Yes	Yes
Anatomical regions studied	Whole brain	Whole brain	Whole brain	Whole brain	Whole brain	Cerebrum and Cerebellum	Whole brain	Brain vasculature and whole brain	Whole brain	Whole brain	Whole brain
Labeling method	Manually labeled on histology, co-registered to MR	Manual on average MR	Manual on an individual, and semi-automatic	Manual on individual MRs	Manual and automatic	Manual on average MR and semi-automatic	Semi-automatic from Kovacevic labels	Manual on average MR	Manual and automatic	Manual on individuals and automatic	Manual on average MR
Number of structures	~70	42	20	13	21	5	42	26	33	33	62
Brain excised or within skull	Within	Excised	Excised	Within skull	Excised	Within skull in-vivo	Excised	Within skull	Within skull	Within skull	Within skull
Focus of study	Anatomical atlas using multiple methods	Variation across individuals	Average atlas and probabilistic atlas	Anatomical and probabilistic neonatal atlas with stereotaxic coordinates	Automatic segmentation of structures, compared with manual	Anatomical abnormality detection in specific structures in mutant	Anatomical differences between strains	Anatomy of cerebral vasculature with reference to brain structures	Automatic segmentation of actively stained MR, vs formalin fixed MR	Baseline atlas of structures focusing on volume, area, and shape	Detailed atlas of mouse brain anatomy

neurobiological research. The brains were scanned post-mortem within the skull, keeping the brain as close to the normal shape as would be found in-vivo. Post-mortem scanning yielded better contrast and image resolution compared to in-vivo methods which are prone to motion artifacts due to breathing and cardiac movements. It also allows for closer placement of MR coils and longer scanning duration (11 h) which is not possible under anaesthesia (3–4 h). Post-mortem scanning thus yields higher resolution images.

Sample preparation

For this study, 40 adult mice (20 males and 20 females) of C57Bl/6J strain were acquired from Charles River, Wilmington, MA. The mice were 12 weeks of age with a mean body weight of 27.4 g±1.2 SD for males and 21.6 g±1.1 SD for females. Animals were anaesthetized with a combination of Ketamine (Pfizer, Kirkland, QC) (100 mg/kg) and Rompun (Bayer Inc., Toronto, ON) (20 mg/kg) via intraperitoneal injection. A previously described sample preparation protocol for scanning was used with slight modifications (Tyszka et al., 2006). Thoracic cavities were opened and animals were perfused through the left ventricle with 30 ml of phosphate buffered saline (PBS) (pH 7.4) at room temperature (25 °C). This was followed by infusion with 30 ml of iced 4% paraformaldehyde (PFA) in PBS. Following perfusion, the heads were removed along with the skin, lower jaw, ears and the cartilaginous nose tip. The remaining skull structures containing the brain were allowed to postfix in 4% PFA at 4 °C for 12 h.

Following an incubation period of 5 days in PBS and 0.01% sodium azide at 15 °C, the skulls were transferred to a PBS and 2 mM ProHance® (Bracco Diagnostics Inc., Princeton, NJ) solution for at least 7 days at 15 °C (Tyszka et al., 2006). MR imaging occurred 12 to 21 days post-mortem. All the animal experiments were approved by the animal ethics committee of the Hospital for Sick Children, Toronto, Ontario.

MR acquisition

A multi-channel 7.0 T MRI scanner (Varian Inc., Palo Alto, CA) with a 6-cm inner bore diameter insert gradient set was used to acquire anatomical images of brains within skulls. Prior to imaging, the samples were removed from the contrast agent solution, blotted and placed into 13 mm diameter plastic tubes filled with a proton-free susceptibility-matching fluid (Fluorinert FC-77, 3M Corp., St. Paul, MN). Three custom-built, 14 mm diameter solenoid coils with a length of 18.3 cm and over wound ends were used to image three brains in parallel. Parameters used in the scans were optimized for grey/white matter contrast: a T2-weighted, 3D fast spin-echo sequence, with TR/TE=325/32 ms, four averages, field-of-view 12×

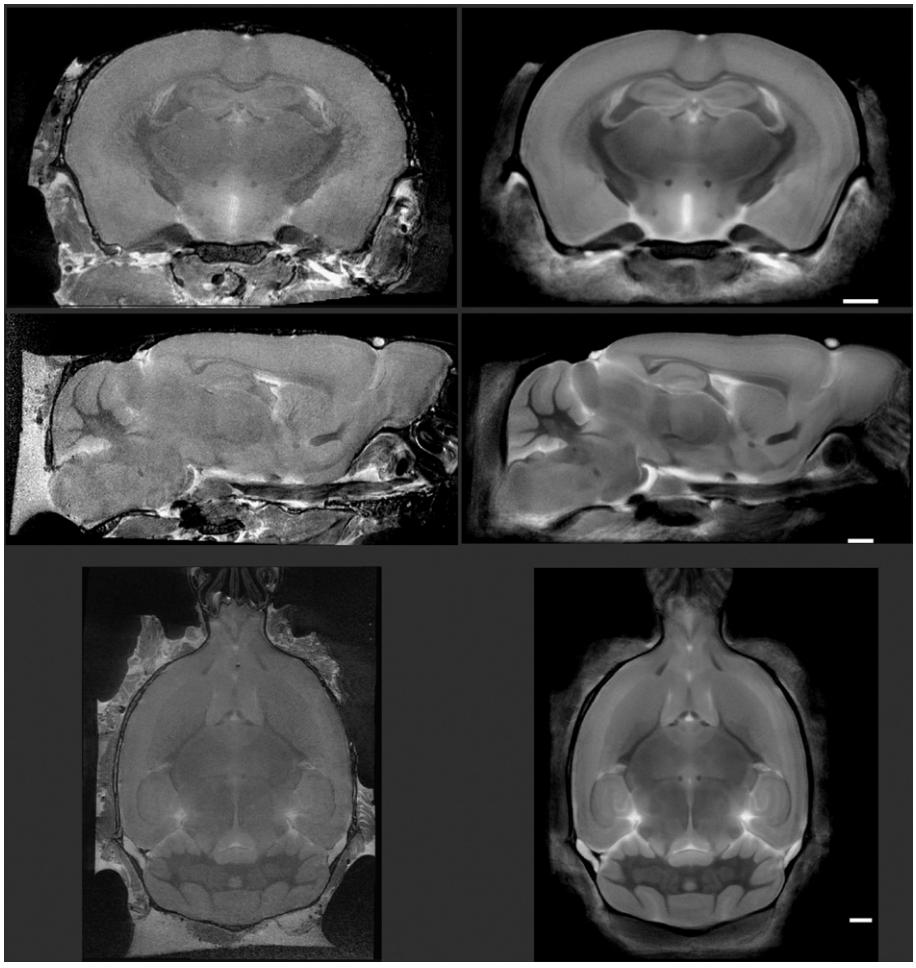

Fig. 1. Represents the resolution of individual mouse brain images (left) in comparison with the average image (right). The average image allowed sharper identification of structures that were otherwise difficult to see on individual brains. Scale bars equal 1 mm.

12×25 mm and matrix size=432×432×780 giving an image with 32 μm isotropic voxels, optimized for image-based registration (Kale et al., in press). Total imaging time was 11.3 h where three brains were scanned simultaneously. It took 14 sessions to complete the scanning of all brains. Geometric distortion due to position of the three coils inside the magnet was corrected using an MR calibration phantom.

Single average volume using 40 mouse brain scans

An unbiased model independent average of the 40 MR scans was created through the following procedure (Kovacevic et al., 2005; Chen et al., 2006). All scans were normalized for intensity inhomogeneities using the N3 method (Sled et al., 1998) and linearly (3 rotations, 3 translations) registered towards a pre-existing atlas. This atlas was only used for the first rigid-body registration (i.e. only global rotations and translations are applied). All possible pair wise 12 parameter registrations (3 scales, 3 shears, 3 rotations, and 3 translations) were then computed, and an average transform created for each mouse. All scans were then averaged to create the first population atlas, representing the average anatomy of the study sample after accounting for overall differences in brain volume. An iterative 6 generation multi scale non-linear alignment procedure was then begun, initially registering each mouse towards the 12 parameter registration atlas, and subsequently towards the atlas of the previous non-linear generation. All registrations were performed using the MNI autoreg tools (Collins et al., 1994), which use an elastic registration algorithm. The end-result is to have all 40 scans deformed into exact alignment with each other in an unbiased fashion (Fig. 1).

Segmentation of brain structures

Using the single average volume of the 40 brain images, bilateral manual segmenting (Fig. 2A) of 62 structures (listed in Table 2) was performed by a single person using the software package Display

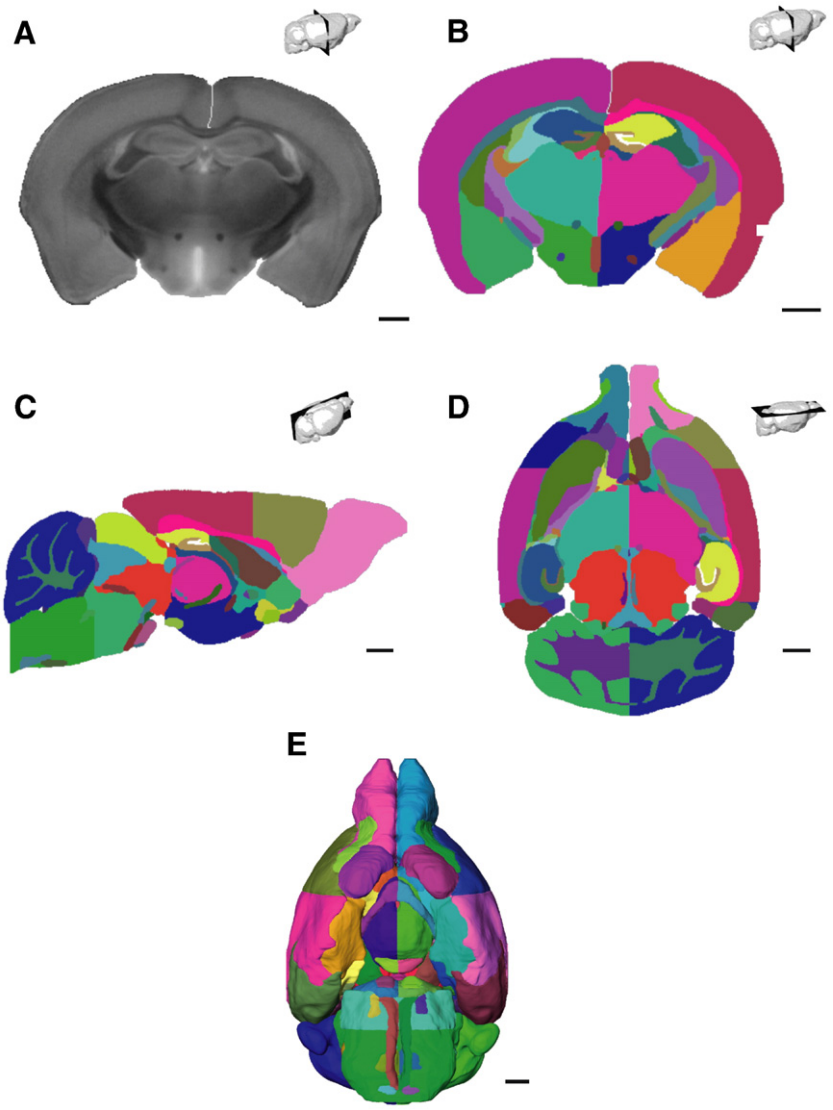

Fig. 2. Labeling of the mouse brain atlas. A coronal slice through MR without labeling is seen in A, while B shows the same coronal slice, after structural labeling for the atlas. Panel C and Fig. 1D show the labeled sagittal and horizontal MR slices, respectively. Panel E shows a three-dimensional representation of the atlas from the inferior view. Scale bars equal 1 mm.

Table 2
List of brain structures with the mean volume±standard deviation (mm^3) calculated using non-linear registration of the average atlas labels to individual mouse brains

Region	Structure	Male (n=20)		Female (n=20)	
		Left	Right	Left	Right
Cerebral grey	Amygdala	7.0±0.54	7.1±0.30	7.0±0.40	6.8±0.53
	Basal forebrain	2.2±0.14	2.2±0.092	2.5±0.62	2.2±0.39
	Bed nucleus of stria terminalis	0.7±0.03	0.7±0.04	0.6±0.04	0.6±0.03
	Caudate/putamen	9.5±0.58	9.8±0.47	9.2±0.68	9.1±0.58
	Entorhinal area	5.9±0.38	5.3±0.25	5.9±0.28	5.2±0.31
	Frontal lobe	20±0.96	19±0.86	25±15	21±1.9
	Occipital lobe	3.2±0.25	3.0±0.25	3.2±0.25	2.9±0.30
	Parieto-temporal lobe	40±2.6	36±2.1	41±2.8	37±3.0
	Dentate gyrus of hippocampus	1.8±0.12	1.9±0.065	1.88±0.21	1.9±0.099
	Fundus of striatum	0.07±0.01	0.07±0.01	0.09±0.04	0.07±0.01
	Globus pallidus	1.5±0.073	1.4±0.073	1.4±0.089	1.3±0.084
	Hippocampus proper	11±0.60	10±0.4	10±0.6	10±0.5
	Hypothalamus	5.4±0.23	5.3±0.24	5.4±0.23	5.3±0.32
	Lateral septal complex	1.6±0.052	1.6±0.070	1.4±0.067	1.5±0.095
	Mammillary bodies	0.3±0.02	0.3±0.02	0.3±0.02	0.3±0.02
	Medial septal complex	0.6±0.05	0.5±0.05	0.6±0.05	0.53±0.07
	Nucleus accumbens	1.9±0.063	1.8±0.083	1.8±0.18	1.8±0.11
	Pre–post-parasubiculum	1.1±0.063	1.2±0.071	1.1±0.071	1.2±0.085
	Stratum granulosum of hippocampus	0.4±0.03	0.5±0.02	0.4±0.04	0.5±0.04
	Thalamus	8.25±0.32	8.4±0.38	7.99±0.29	8.0±0.48
Cerebral white	Anterior part of anterior commissure	0.6±0.03	0.7±0.03	0.6±0.05	0.7±0.04
	Posterior part of anterior commissure	0.2±0.01	0.2±0.01	0.2±0.04	0.2±0.01
	Posterior commissure	0.1±0.01		0.1±0.01	
	Cerebral peduncle	1.1±0.083	1.1±0.060	1.0±0.043	1.1±0.070
	Corpus callosum	8.7±0.55	8.2±0.49	8.4±0.47	7.9±0.59
	Fasciculus retroflexus	0.1±0.01	0.1±0.01	0.1±0.01	0.1±0.01
	Fimbria	1.7±0.21	1.5±0.10	1.5±0.075	1.4±0.096
	Fornix	0.3±0.02	0.3±0.02	0.3±0.02	0.3±0.02
	Habenular commissure	0.02±0.002	0.01±0.002	0.02±0.003	0.01±0.003
	Internal capsule	1.3±0.16	1.3±0.066	1.2±0.069	1.2±0.086
	Mammillothalamic tract	0.1±0.01	0.1±0.01	0.1±0.01	0.1±0.01
	Optic tract	0.9±0.2	0.8±0.05	1±0.7	0.8±0.05
	Stria medullaris	0.3±0.02	0.4±0.02	0.3±0.02	0.4±0.02
	Stria terminalis	0.5±0.04	0.4±0.02	0.5±0.04	0.4±0.04
Olfactory	Olfactory bulbs	12±0.43	12±0.52	12±0.62	12±0.57
	Olfactory tubercle	1.6±0.093	1.7±0.17	1.9±0.26	1.9±0.27
	Lateral olfactory tract	0.6±0.04	0.6±0.03	0.7±0.1	0.7±0.07
	Subependymal zone/rhinocele	0.04±0.003	0.03±0.002	0.04±0.004	0.03±0.002
Cerebellum	Arbor vita of cerebellum	5.2±0.23	5.2±0.23	5.2±0.28	5.1±0.21
	Cerebellar cortex	25±1.5	25±1.0	26±1.4	25±1.4
	Inferior cerebellar peduncle	0.4±0.02	0.4±0.01	0.4±0.02	0.4±0.02
	Middle cerebellar peduncle	0.6±0.03	0.6±0.02	0.7±0.08	0.6±0.04
	Superior cerebellar peduncle	0.5±0.04	0.5±0.02	0.5±0.03	0.4±0.03
Ventricles	Lateral ventricle	2.0±0.83	2.1±0.50	1.8±0.30	2.1±0.55
	Third ventricle	1.3±0.23		1.4±0.14	
	Cerebral aqueduct	0.6±0.1		0.6±0.01	
	Fourth ventricle	0.5±0.1		0.5±0.05	
Brainstem	Inferior colliculus	2.8±0.12	2.7±0.11	2.7±0.11	2.7±0.12
	Superior colliculus	4.0±0.15	4.0±0.16	3.8±0.14	3.8±0.19
	Corticospinal tract/pyramid	0.8±0.04	0.7±0.04	0.8±0.04	0.77±0.04
	Cuneate nucleus	0.1±0.01	0.1±0.02	0.1±0.02	0.2±0.01
	Facial nerve	0.1±0.01	0.1±0.003	0.1±0.01	0.1±0.01
	Inferior olivary complex	0.2±0.01	0.2±0.02	0.2±0.02	0.2±0.02
	Medial lemniscus/medial longitudinal fasiculus	1.3±0.05	1.3±0.05	1.3±0.06	1.2±0.07
	Pontine nucleus	0.4±0.03	0.4±0.03	0.4±0.04	0.4±0.03
	Superior olivary complex	0.4±0.02	0.4±0.02	0.4±0.02	0.4±0.01
	Periaqueductal grey	3.9±0.14		3.6±0.15	
	Medulla	26±0.75		26±1.1	
	Midbrain	13±0.58		12±0.58	

(continued on next page)

Table 2 (*continued*)

Region	Structure	Male (n=20)		Female (n=20)	
		Left	Right	Left	Right
Brainstem	Pons	16±0.42		15±0.51	
	Interpeduncular nucleus	0.2±0.02		0.2±0.01	
	Ventral tegmental decussation	0.1±0.01		0.1±0.01	

(http://www.bic.mni.mcgill.ca/software/Display/Display.html, Montreal Neurological Institute, Montreal, Canada). The majority of the structures were initially segmented slice by slice along the coronal orientation paying close attention to the other two orientations, as well as to the slices preceding and following throughout the segmentation process. Some structures, however, were initially segmented primarily along the horizontal or sagittal orientations, depending on which orientation was clearest for the structure shape. The largest and most well defined structures (such as the thalamus, cortex, caudate/putamen and corpus callosum) were segmented first, as their boundaries help to define the nearby smaller structures with less well defined boundaries. After each structure was labeled, the boundaries were carefully checked again for any mislabeling and any corrections required were made using all three orientations.

A two-dimensional representation of the atlas in three orientations is shown in Figs. 2B–D; a three-dimensional representation of the atlas from the inferior view is shown in Fig. 2E. The nomenclature protocol used in this atlas was based on the University of Washington NeuroNames (http://braininfo.rprc.washington.edu/menumain.html) which is a standardized brain nomenclature created by Bowden and Martin (1995). NeuroNames incorporates rodent atlases from Paxinos and Franklin (2001), Hof et al. (2000), Swanson (2004), A.I.B.S. and Dong (2008). The guidelines for the location and boundaries of structures were obtained using the Allen

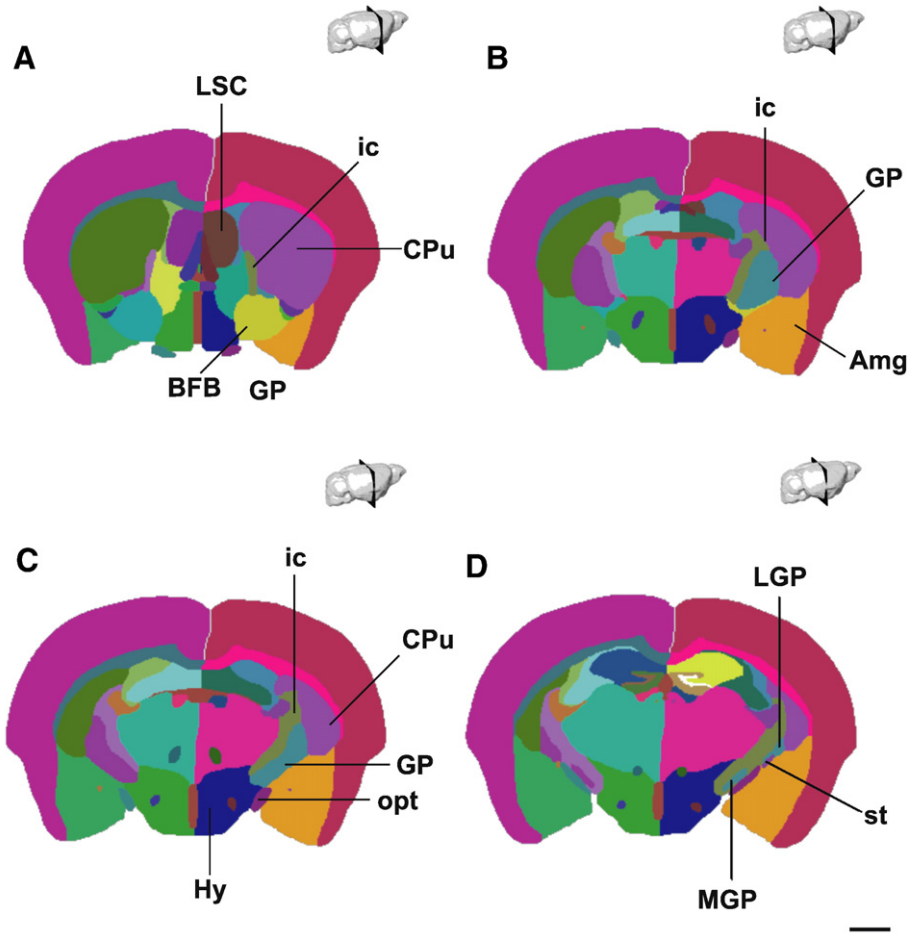

Fig. 3. Represents coronal slices through the globus pallidus (GP). Panel A is the anterior aspect of the GP while B is the thickest portion of GP. As the GP extends posteriorly, it thins out and elongates, as seen in C. The posterior aspect of the GP is shown in D. Scale bars equal 1 mm. Amg = amygdala, BFB = basal forebrain, CPu = caudate and putamen, GPL = globus pallidus lateral, Hy = hypothalamus, ic = internal capsule, GPM = globus pallidus medial, LSC = lateral septal complex, opt = optic tract, st = stria terminalis.

Reference Atlas available online at http://www.brain-map.org/ (Lein et al., 2007), Sidman et al.'s High Resolution Mouse Brain Atlas available online at http://www.hms.harvard.edu/research/brain/atlas.html and Paxinos and Franklin (2001).

Structure boundary descriptions

A detailed boundary description for each of the 62 brain structures is available in the Supplementary data section. Each region is described by defining the anterior–posterior, superior–inferior and lateral–medial relationships with other surrounding structures. Here we give a single example.

Globus pallidus

The anterior extreme of the globus pallidus (the right globus pallidus is labeled cobalt blue) begins one coronal slice prior to the final slice showing the anterior commissure decussation (Fig. 3A), along the medial–inferior aspect of the caudate/putamen (light purple). At this point, the boundaries are the internal capsule (olive green) medially, the caudate/putamen superio-laterally, the posterior part of the anterior commissure (eggplant) anteriorly, and the basal forebrain (yellow) inferio-medially.

The globus pallidus expands laterally along the inferior aspect of the caudate/putamen; the inferio-lateral edge briefly touches the posterior part of the anterior commissure and the fundus of striatum (green). Both these structures quickly shift laterally away as the inferio-lateral border becomes occupied by the basal forebrain. Soon after, the basal forebrain shrinks, receding from the inferio-lateral border to reveal the amygdala (pumpkin) as the new border in this region. Meanwhile, the internal capsule grows superiorly, curving over the superior aspect of the globus pallidus (Fig. 3B).

The basal forebrain vanishes at one to three slices prior to the disappearance of the lateral septal complex (brown) and the hypothalamus (indigo) occupies the inferio-medial boundary of the globus pallidus. The globus pallidus then elongates into a thin structure at five to six slices posterior and the caudate/putamen now lies lateral to the globus pallidus (Fig. 3C). The optic tract (red–violet) gradually moves along the inferio-lateral edge of the globus pallidus; meanwhile the stria terminalis (violet) shifts from within the amygdala toward the globus pallidus, eventually bordering the inferio-lateral aspect immediately superior to the optic tract location. Continuing four slices posteriorly, the globus pallidus splits into a medial and lateral portion (Fig. 3D). The medial globus pallidus is surrounded superiorly, medially, and inferiorly by the internal capsule, while the optic tract lies inferio-laterally. The medial portion of the globus pallidus quickly shrinks away from the optic tract (two to four slices posteriorly), and the cerebral peduncle (dark green) is found directly posterior to the medial globus pallidus. The lateral globus pallidus is

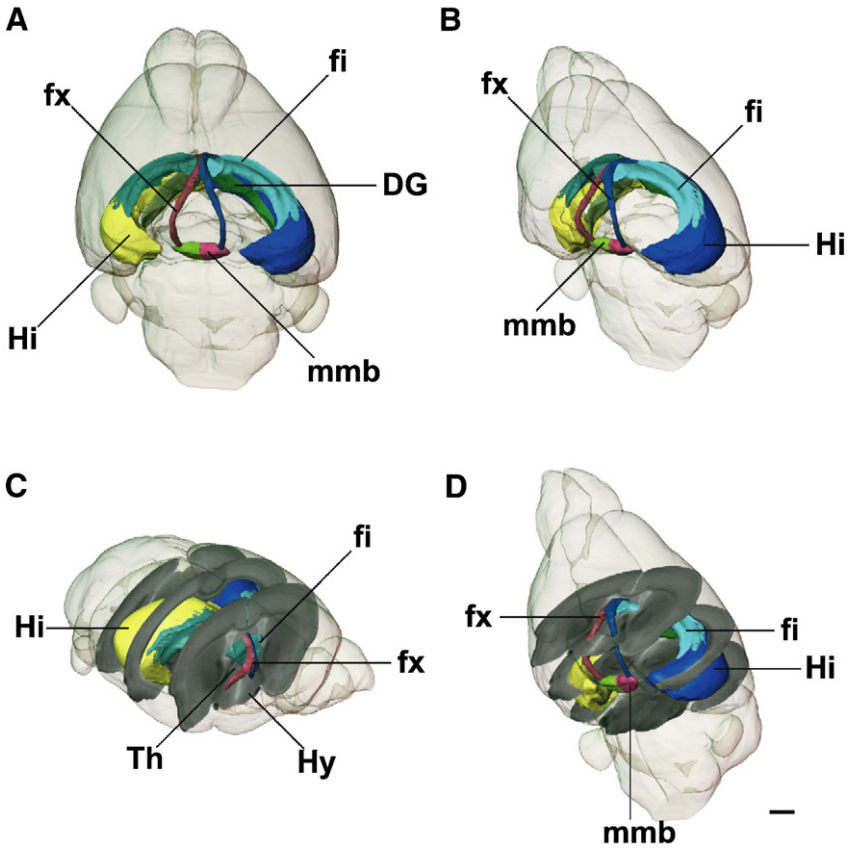

Fig. 4. Shows the hippocampus, fimbria, fornix and mammillary bodies in a three-dimensional transparent brain. Panels A and B show the fornix extending from the fimbria and hippocampus, to the mammillary bodies as seen from the anterior–inferior and left-inferior views, respectively. Panel C which is the anterior-right and the left-inferior views shows the same structures through MR slices along the anterior, middle, and posterior regions of the structural complex of interest. The fornix can be seen extending inferiorly and anterior to the thalamus, and then posteriorly through the hypothalamus toward the mammillary bodies. Scale bars equal 1 mm. DG = dentate gyrus of hippocampus, fi = fimbria, fx = fornix, Hi = hippocampus, Hy = hypothalamus, Mmb = mammillary body, Th = thalamus.

bounded laterally by the amygdala and caudate/putamen, medially and superiorly by the internal capsule, and inferio-laterally by the stria terminalis. The lateral globus pallidus disappears two to four slices posterior and the caudate/putamen and internal capsule appear directly posterior to the lateral globus pallidus.

Results

The process described above resulted in a neuroanatomical atlas consisting of 62 structures (Table 2), which will be freely available to the research community. Based on the average mouse atlas presented in this paper, the volume for each individual mouse brain was computed by integrating over the Jacobian determinants for each voxel that belongs to a structure. This process is equivalent to resampling the atlas towards each mouse brain in native MRI space and getting the volume of the resampled labels. Using this semi-automated technique, Table 2 describes the mean volumes of various structures in each of the two hemispheres in male and female sub-groups of our sample.

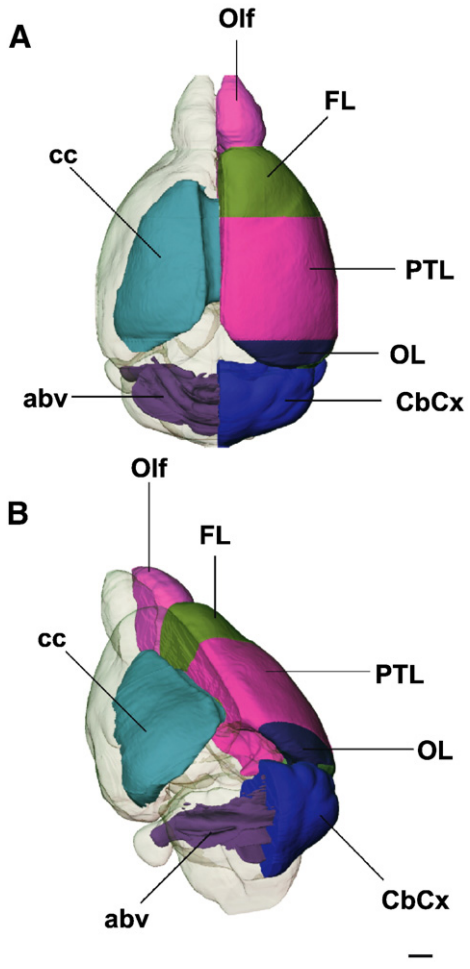

Fig. 5. Represents the cortex and underlying white matter in a three-dimensional transparent brain from A) the top view, and B) the back left view. The cortex has been removed from the left hemisphere to show the underlying white matter. Scale bar equals 1 mm. abv = arbor vitae of cerebellum, CbCx = cerebellar cortex, cc = corpus callosum, FL = frontal lobe, OL = occipital lobe, PTL = parieto-temporal lobe, Olf = olfactory bulb.

This atlas allows for the visualization of complex relationships between anatomical structures. Two illustrative examples are provided below: the first example is the 3D relationship between the fornix, fimbria, hippocampus and mammillary bodies (Fig. 4). The fimbria of the fornix is white matter, attached to the hippocampus. The fimbria condenses along the midline, becoming the body of the fornix. The body of the fornix descends anterior to the thalamus, slightly separating from the midline as it nears the anterior commissure decussation. The fornix embeds within the hypothalamus; meanwhile the fornix takes a sharp turn posteriorly, heading toward the mammillary bodies where the fornix ends.

Fig. 5 shows a superior view of the cortex and underlying white matter. The cerebral cortex and the cerebellum are shown intact in the right hemisphere. In the left hemisphere, the cortex is removed to reveal the corpus callosum and arbor vita; the white matter regions lying immediately beneath the cerebral and cerebellar cortex, respectively.

Discussion

The atlas constitutes 62 structures that were clear to view at the resolution of 32 μm, with the smallest structure being the habenular commissure. Some structures which are described by their individual sub-components in histological atlases (Hof et al., 2000; Paxinos and Franklin, 2001; Swanson, 2004; Lein et al., 2007; Dong, 2008), but were indecipherable at this resolution are presented as aggregates, such as the amygdala, the thalamus and the hypothalamus. Similarly, the histological atlases describe the cytoarchitectural maps of the cortex rather than divide them into lobes. Since this was not a possibility in our images, we have used the deeper brain structures to define the boundaries of cortical lobes.

The Supplementary data of this paper lists the acronyms used in this and other atlases which should allow users to compare the regions of interests here with those described by other researchers.

Comparison with histological atlases

While the total number of 62 structures defined in this atlas is fewer than the number of structures reported previously in histological atlases (Hof et al., 2000; Paxinos and Franklin, 2001), it is the largest number of structures to date to be manually traced directly on a mouse MR image itself. Histological atlases have an advantage of being at a higher resolution than mouse MR atlases and staining techniques can be applied directly to the histological slices to enhance structural boundaries, thus allowing visualization of finer regions than can be seen in our atlas. Depending on the type of study undertaken, however, an MR atlas could be more appropriate for a number of reasons. Most importantly the use of an MRI based atlas allows for newly acquired MR images to be registered to the atlas and structure labels on the atlas to be back-propagated on to the images. Furthermore, if 3D spatial relationships and distances between neuroanatomical structures are of interest, one can examine this directly via an MR image: the shape and size of the structures are anatomically conserved as would be found in-vivo in the whole mouse brain, especially if the brain is enclosed within the skull during the scanning process. Structural volumes can be easily and reliably extracted from MR images, something that is simply not practical with histological atlases. It is possible to create a 3D volume from 2D histological sections (Ju et al., 2006), however the methods are complicated. As each histological section may have varying degrees of tissue distortion; such as artifacts, elongation, shrinkage, and spatial shifting. While the

results of converting a 2D histological image into 3D are interesting in a descriptive sense, such reconstructed images cannot be used reliably for volumetric measurements and moreover, the structural shapes appear altered or distorted from the shape seen in-situ. In addition, the resulting volume is based on a single mouse brain rather than the average of several.

Comparison with other MRI based atlases

Our atlas was created by manually segmenting the identifiable structures directly onto the average MRI. It is possible to co-register a previously defined histological atlas onto an MR scan, thereby saving the labor of manual segmentation. In one such study, the Paxinos and Watson rat brain atlas was registered to a rat MR, however, the number of coronal slices for the atlas was fewer than the number of coronal slices on the MR; the histological atlas slices were therefore repeated in order to fit completely on the MR image (Schwarz et al., 2006). In addition, some spatial alignment challenges become evident when one co-registers brain slices obtained from separate mice through two very different modalities. For example, in one study the midbrain and colliculi proved difficult to align (Schwarz et al., 2006).

MacKenzie-Graham et al. created a mouse atlas using histologically stained slices and co-registered those to the MR images from the same mouse, thereby reducing some alignment issues, (MacKenzie-Graham et al., 2004).

Manual structure segmentation was performed directly on mouse MRI in several studies, either on individual brains (Redwine et al., 2003; Kovacevic et al., 2005; Lee et al., 2005; Ma et al. 2005; Bock et al., 2006; Dorr et al., 2007) or on average MR images (Kovacevic et al., 2005; Bock et al., 2006; Dorr et al., 2007). The atlases created by Ma et al. (2005) and from the Johnson group (Ali et al., 2005; Badea et al., 2007a; Sharief et al., 2008), use the same mouse strain as in our study; however, there exist several key differences with our atlas. First, their segmentation of 20–33 structures was performed on individual brains. In the case of Ma et al., a single artifact-free brain was manually segmented as a representative of the ten mouse brains scanned. The remaining brains in their study were semi-automatically segmented using the representative brain's segmentation, after which point the ten segmented atlases were combined to form an average atlas and a probabilistic atlas of the ten brains. The atlases from the Johnson group were created from automatically segmented individual brains based on a protocol developed in Ali et al. (2005) where in each study, the automatic segmentation was validated by comparisons with manual tracings of the same MR volumes. In our atlas, the manual segmentation of 62 structures was performed on an average MR of 40 mouse brains, which factors out the occurrence of artifacts as would be seen on individual brains and increases the clarity of the image for improved structural boundary determination for even the small brain structures. Only a few highly variable structures, such as vasculature and white matter striations in the caudate-putamen, are factored out in an averaged image (Kovacevic et al., 2005); striation patterning could be better studied on an individual representative brain and same is true for basic cerebrovascular anatomy (Dorr et al., 2007).

The Ma and the Johnson groups used a total of 6–12 male mice, while our group scanned 20 male and 20 female mice as it has been shown recently that male and female C57Bl/6J mice show sexual dimorphism in relation to overall brain and individual structure size (Spring et al., 2007). In addition, Ma's atlas used excised mouse brains, resulting in shape changes in certain susceptible regions such as the olfactory bulb, cerebellum, brainstem, and cortex when compared to brains scanned within skull. To avoid this, our group scanned the brains within skull, thus conserving the natural shape of the mouse brain.

Applications and limitation

While the resolution of our T2 MR images is considerably higher than that reported in other atlases, it is not comparable to that seen in histological atlases. As such, the boundaries between structures are not as precise as could be achieved with histological studies. Image resolution in MR limits the delineation of smaller structures like the individual hypothalamic nuclei, the various parts of the amygdala, and subdivisions of the hippocampus. Thus the resolution obtained through the MR imaging protocol employed in this study, while unrivaled in terms of MR mouse neuroanatomy atlases, still falls short of the in-plane resolution obtainable by histology. There is thus some motivation for aligning histology slices with MR images in order to obtain three-dimensional stacks of these slices upon which an atlas could be based. The main challenges are accurately aligning the individual slices to the MR, accounting for the tissue distortion introduced by the preparation of specimen for histology, and being able to combine the histology information into averages representing multiple mice.

Indeed these limitations hinder the usage of MR for identification of some structures; however, there are several other structures that can be visualized in great detail in this atlas. Thus, it would be useful for researchers working with MR to be able to refer to an atlas created from a similar modality and oriented in a common coordinate system. Since it has been reported that the quality of automatic segmentation is comparable to that of manual segmentation (Ali et al., 2005; Badea et al., 2007a; Sharief et al., 2008), this atlas could also be used as a template for automatic segmentation of brain images in future studies. However, it is important to note that the shape of structures may differ between strains. Chen et al., explored the differences in neuroanatomy within strains and between strains, including the C57Bl/6J strain (Chen et al., 2006). Using MR-based techniques, they found more differences in volumes and structural position between strains than within strains. Therefore, the atlas described for this paper may exhibit some differences from strains other than the C57Bl/6J mouse. However the spatial organization of the structures and pattern of anatomical relationships does not differ severely between strains and hence this atlas is usable for the general guidance purpose of brain anatomy in strains other than C57B1/6J.

When segmenting structures on an MR image for volumetrics, it could be beneficial to paint the same structures a number of times, assessing reliability of segmentation and/or to average the segmented volumes together to form one median atlas. While the atlas presented here is created by painting structures only once on a single average atlas, it should be noted that the structures were assessed multiple times for accuracy of boundary limits, corrected in all three orientations, and verified with available histological atlases.

Conclusion

The atlas created here is intended for general neuroanatomical guidance; in other words to assist in finding structure locations, understanding three-dimensional relationships in mouse neuroanatomy, and for structural segmentation techniques. It could be useful to co-register the atlas to other mouse brains for aid in segmentation

when needed; however, some adjustments may need to be made to the final product as the labels may not fit perfectly, especially when registered to individual brains and to strains other than C57Bl/6J. We expect that this freely available atlas will be of great utility to the researchers.

Acknowledgments

The authors would like to thank the Sunnybrook Health Sciences Support Funds and the Ontario Research and Development Challenge Fund Grant.

Appendix A. Supplementary data

Supplementary data associated with this article can be found, in the online version, at doi:10.1016/j.neuroimage.2008.03.037.

References

A.I.B.S., Allen Brain Atlas Internet — www.brain-map.org.

Ali, A.A., Dale, A.M., Badea, A., Johnson, G.A., 2005. Automated segmentation of neuroanatomical structures in multispectral MR microscopy of the mouse brain. NeuroImage 27, 425–435.

Anderson, S.A., Frank, J.A., 2007. MRI of mouse models of neurological disorders. NMR Biomed. 20, 200–215.

Badea, A., Ali-Sharief, A.A., Johnson, G.A., 2007a. Morphometric analysis of the C57BL/6J mouse brain. NeuroImage 37, 683–693.

Badea, A., Nicholls, P.J., Johnson, G.A., Wetsel, W.C., 2007b. Neuroanatomical phenotypes in the reeler mouse. NeuroImage 34, 1363–1374.

Benveniste, H., Blackband, S.J., 2006. Translational neuroscience and magnetic-resonance microscopy. Lancet Neurol. 5, 536–544.

Bock, N.A., Kovacevic, N., Lipina, T.V., Roder, J.C., Ackerman, S.L., Henkelman, R.M., 2006. In vivo magnetic resonance imaging and semi-automated image analysis extend the brain phenotype for cdf/cdf mice. J. Neurosci. 26, 4455–4459.

Bowden, D.M., Martin, R.F., 1995. NeuroNames Brain Hierarchy. NeuroImage 2, 63–83.

Chen, X.J., Kovacevic, N., Lobaugh, N.J., Sled, J.G., Henkelman, R.M., Henderson, J.T., 2006. Neuroanatomical differences between mouse strains as shown by high-resolution 3D MRI. NeuroImage 29, 99–105.

Collins, D.L., Neelin, P., Peters, T.M., Evans, A.C., 1994. Automatic 3D intersubject registration of MR volumetric data in standardized Talairach space. J. Comput. Assist. Tomogr. 18, 192–205.

Dong, H., 2008. The Allen Reference Atlas: a Digital Colour Brain Atlas of C57BL/6J Male Mouse. John Wiley & Sons, Inc., New Jersey.

Dorr, A., Sled, J.G., Kabani, N., 2007. Three-dimensional cerebral vasculature of the CBA mouse brain: a magnetic resonance imaging and micro computed tomography study. NeuroImage 35, 1409–1423.

Hof, P.R., Young, W.G., Bloom, F.E., Belichenko, P.V., Celio, M.R., 2000. Comparative cytoarchitectonic atlas of the C57BL/6 and 129/Sv mouse brains. Elsevier, Amsterdam.

Ju, T., Warren, J., Carson, J., Bello, M., Kakadiaris, I., Chiu, W., Thaller, C., Eichele, G., 2006. 3D volume reconstruction of a mouse brain from histological sections using warp filtering. J. Neurosci. Methods 156, 84–100.

Kale, S.C., Lerch, J.P., Henkelman, R.M., Chen, X.J., in press. Optimization of the SNR-resolution tradeoff for registration of magnetic resonance images. Hum. Brain Mapp. doi:10.1002/hbm.20453.

Kovacevic, N., Henderson, J.T., Chan, E., Lifshitz, N., Bishop, J., Evans, A.C., Henkelman, R.M., Chen, X.J., 2005. A three-dimensional MRI atlas of the mouse brain with estimates of the average and variability. Cereb. Cortex 15, 639–645.

Lee, E.F., Jacobs, R.E., Dinov, I., Leow, A., Toga, A.W., 2005. Standard atlas space for C57BL/6J neonatal mouse brain. Anat. Embryol. (Berl.) 210, 245–263.

Lein, E.S., Hawrylycz, M.J., Ao, N., Ayres, M., Bensinger, A., Bernard, A., Boe, A.F., Boguski, M.S., Brockway, K.S., Byrnes, E.J., Chen, L., Chen, L., Chen, T.M., Chin, M.C., Chong, J., Crook, B.E., Czaplinska, A., Dang, C.N., Datta, S., Dee, N.R., Desaki, A.L., Desta, T., et al., 2007. Genome-wide atlas of gene expression in the adult mouse brain. Nature 445, 168–176.

Ma, Y., Hof, P.R., Grant, S.C., Blackband, S.J., Bennett, R., Slatest, L., McGuigan, M.D., Benveniste, H., 2005. A three-dimensional digital atlas database of the adult C57BL/6J mouse brain by magnetic resonance microscopy. Neuroscience 135, 1203–1215.

MacKenzie-Graham, A., Lee, E.F., Dinov, I.D., Bota, M., Shattuck, D.W., Ruffins, S., Yuan, H., Konstantinidis, F., Pitiot, A., Ding, Y., Hu, G., Jacobs, R.E., Toga, A.W., 2004. A multimodal, multidimensional atlas of the C57BL/6J mouse brain. J. Anat. 204, 93–102.

Nieman, B.J., Bock, N.A., Bishop, J., Chen, X.J., Sled, J.G., Rossant, J., Henkelman, R.M., 2005. Magnetic resonance imaging for detection and analysis of mouse phenotypes. NMR Biomed. 18, 447–468.

Paxinos, G., Franklin, K., 2001. The Mouse Brain in Stereotaxic Coordinates. Acedemic Press, San Diego, CA.

Redwine, J.M., Kosofsky, B., Jacobs, R.E., Games, D., Reilly, J.F., Morrison, J.H., Young, W.G., Bloom, F.E., 2003. Dentate gyrus volume is reduced before onset of plaque formation in PDAPP mice: a magnetic resonance microscopy and stereologic analysis. Proc. Natl. Acad. Sci. U. S. A. 100, 1381–1386.

Schwarz, A.J., Danckaert, A., Reese, T., Gozzi, A., Paxinos, G., Watson, C., Merlo-Pich, E.V., Bifone, A., 2006. A stereotaxic MRI template set for the rat brain with tissue class distribution maps and co-registered anatomical atlas: application to pharmacological MRI. NeuroImage 32, 538–550.

Sharief, A.A., Badea, A., Dale, A.M., Johnson, G.A., 2008. Automated segmentation of the actively stained mouse brain using multi-spectral MR microscopy. NeuroImage 39 (1), 136–145.

Sled, J.G., Zijdenbos, A.P., Evans, A.C., 1998. A nonparametric method for automatic correction of intensity nonuniformity in MRI data. IEEE Trans. Med. Imag. 17, 87–97.

Spring, S., Lerch, J.P., Henkelman, R.M., 2007. Sexual dimorphism revealed in the structure of the mouse brain using three-dimensional magnetic resonance imaging. NeuroImage 35, 1424–1433.

Swanson, L., 2004. Brain Maps: Structure of the Rat Brain. Elsevier, Amsterdam.

Tyszka, J.M., Readhead, C., Bearer, E.L., Pautler, R.G., Jacobs, R.E., 2006. Statistical diffusion tensor histology reveals regional dysmyelination effects in the shiverer mouse mutant. NeuroImage 29, 1058–1065.